Computer Simulation Studies of Aβ 37−42 Aggregation Thermodynamics and Kinetics in Water and Salt Solution

ARTICLE *in* THE JOURNAL OF PHYSICAL CHEMISTRY B · MAY 2014

Impact Factor: 3.3 · DOI: 10.1021/jp502169b · Source: PubMed

2 AUTHORS:

Yi Isaac Yang
University of Lugano
8 PUBLICATIONS **4** CITATIONS
SEE PROFILE

Yi Qin Gao
Peking University
98 PUBLICATIONS **2,015** CITATIONS
SEE PROFILE

THE JOURNAL OF PHYSICAL CHEMISTRY B

Article

pubs.acs.org/JPCB

Computer Simulation Studies of Aβ_{37-42} Aggregation Thermodynamics and Kinetics in Water and Salt Solution

Y. Isaac Yang[†] and Yi Qin Gao*[,†]

[†]Institute of Theoretical and Computational Chemistry, College of Chemistry and Molecular Engineering, Peking University, Beijing 100871, China

Supporting Information

ABSTRACT: In vivo self-assembly of proteins into aggregates known as amyloids is related to many diseases. Although a large number of studies have been performed on the formation of amyloid, the molecular mechanism of polypeptide aggregation remains largely unclear. In this paper, we studied the aggregation of amyloid-forming peptide Aβ_{37-42} using all-atom molecular dynamics simulations. Using the integrated temperature sampling (ITS) simulation method, we observed the reversible formation of Aβ_{37-42} oligomers. The free-energy landscape for the polypeptide association was calculated, and aggregated states were then defined based on the landscape. To explore the kinetics and especially salt effects on the process of polypeptide aggregation, normal MD simulations were performed in pure water and NaCl solution, respectively. We then used the transition path theory (TPT) to analyze the transition network of polypeptide aggregation in solution. The dominant pathways of Aβ_{37-42} aggregation were found to differ significantly in pure water and the salt solution, indicating the change of molecular mechanism of polypeptide aggregation with the solution conditions.

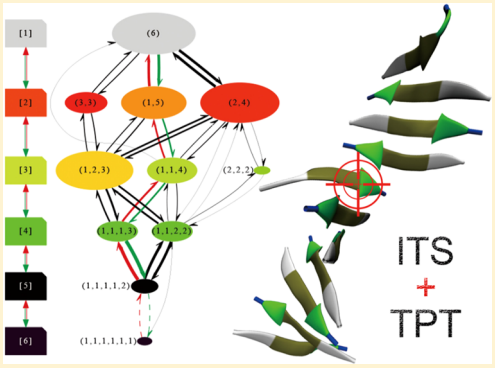

INTRODUCTION

In vivo self-assembly of protein into insoluble fibril aggregates known as amyloids is related to more than 20 severe diseases including diabetes mellitus type II and Alzheimer's and Parkinson's disease.[1,2] Among them, the abnormal aggregate of beta-amyloid (Aβ) is the main component of senile plaques, a type of deposit in the gray matter of the brains of patients with Alzheimer's disease.[3−9] One of the beta-amyloids that has been widely studied is Aβ_{42}, a self-associating polypeptide with high neurotoxicity.[10−12] Studies have shown that the C-terminus of Aβ_{42} has an important effect on the formation of its aggregate.[13−15]

Structures of amyloid fibrils have been revealed by experimental techniques, such as X-ray diffraction and NMR. The proteins in fibrils are organized in a characteristic "cross-β" structure, in which the polypeptides form β-strands oriented perpendicular to the fibril axis.[16,17] Sawaya et al. reported more than 30 crystal structures of aggregated segments of fibril-forming proteins that from amyloid fibrils and classified them into eight classes of "steric zippers" according to their structural features.[18] For instance, the steric zipper of peptide GGVVIA, a sequence from the C-terminal segment of Aβ_{42}, belongs to class 4, which has a parallel arrangement in sheets and a "face-to-back" and "up−down" structure in strands. However, amyloid structures often exhibit polymorphism.[19−21] Berryman et al. have shown that a number of peptides, for example, GNNQQNY, SSTSAA, and GGVVIA,[22] can retain their ordered cross-β architecture characteristic of an amyloid in more than one class of steric zippers structure.

A few studies used the "bottom-up" simulations to investigate the aggregation process from the dispersed polypeptide monomers. Because of the large size of the systems, many studies used coarse-grained (CG) models.[23−27] Mu and Gao investigated the spontaneous formation of the aggregation of peptide Aβ_{37-42} using Monte Carlo simulations and a CG model.[28] A cross-β structure was observed in which parallel β-sheets order into a left-handed helix. In general, using all-atom models in the aggregation simulations remains challenging, but there do exist successful examples. For instance, Baftizadeh et al. performed bias-exchange metadynamics (BE-META) simulations to obtain the aggregated structures of 18 chains of polyvaline[29] and Aβ_{35-40}.[30] In a recent study, Nguyen et al. studied the polymorphism of the aggregation of peptide Aβ_{37-42} using an unbiased replica exchange molecular dynamics (REMD) simulation.[31]

Although, as mentioned above, a large number of studies have been aimed at understanding the mechanism of amyloid self-assembly, the molecular mechanism of polypeptide aggregation is still unclear. Furthermore, the formation of amyloid fibrils can be significantly influenced by solution

Special Issue: William L. Jorgensen Festschrift

Received: March 3, 2014
Revised: May 16, 2014

   dx.doi.org/10.1021/jp502169b | J. Phys. Chem. B XXXX, XXX, XXX−XXX

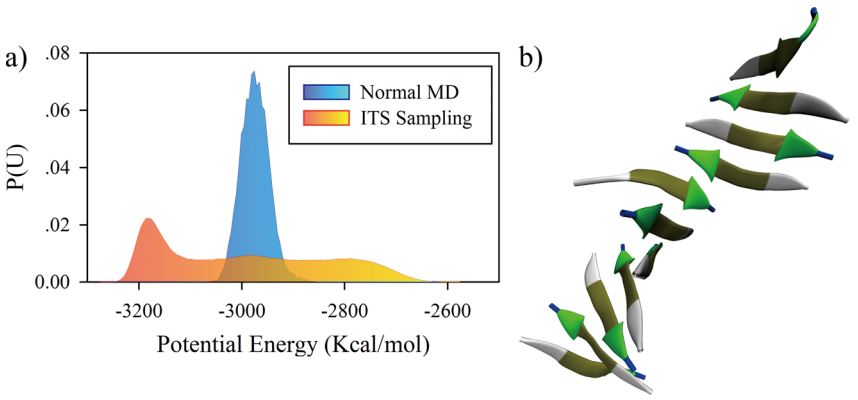

Figure 1. (a) The potential energy distribution and (b) an aggregated structure containing 11 monomers from the ITS-enhanced simulation of Aβ_{37-42} in implicit solvent. The color in the β-strand model means the class of residue: white is glycine (G), tan is valine (V), green is isoleucine (I), and blue is alanine (A).

conditions.[32−34] For example, it is known that NaCl accelerates the aggregation of amyloid in solution.[35] However, the multiple complex pathways in polypeptide aggregation make molecular understanding of its kinetics difficult, and quantitative characterization of the solvent effect is rare. The Markov state models (MSMs)[36−42] were shown to be a promising method for the investigation of the amyloid aggregation kinetics.[25,29,43−46] For example, Qiao et al.[47] used MSMs to study the conformational dynamics of the intrinsically disordered amyloid peptide hIAPP from extensive REMD simulations. In addition, the transition path theory (TPT) can be used in association with MSMs to analyze the statistical properties of a reactive trajectory between the prespecified beginning and ending states.[48−52]

In this study, we investigated the aggregation of hexapeptide Aβ_{37-42}, a segment with the sequence Gly-Gly-Val-Val-Ile-Ala from the C-terminus of Alzheimer's Aβ_{42} amyloid peptide, using all-atom molecular dynamics (MD) simulations. First, we used the integrated temperature sampling (ITS) method[53,54] to study the reversible structure formation and obtain the thermodynamic information on polypeptide association and amyloid aggregation. Then, normal MD simulations were performed in pure water and NaCl solution to investigate the kinetics of polypeptide aggregation and its solution dependence. We used TPT to analyze the detailed pathways of Aβ_{37-42} aggregation.

METHOD

To sample effectively the structures of relatively large aggregations, the ITS-enhanced sampling[53,54] thermodynamics simulation was used. The ITS method generates a broad distribution as a function of the potential energy U of the system, which is achieved by using an effective potential energy U'

$$U' = -\frac{1}{\beta_0}\ln\sum_{N}^{k=1} n_k e^{-\beta_k U} \tag{1}$$

in which β_0 is the temperature of the system of interest, β_k is a series of temperatures that cover both low and high temperatures, and n_k's are reweighting factors obtained through an iterative procedure. The thermodynamic properties of the system, such as the free-energy landscape calculated in this paper, are then calculated by the following reweighting factors

$$e^{-\beta_0(U-U')} = \frac{e^{-\beta_0 U}}{\sum_{N}^{k=1} n_k e^{-\beta_k U}} \tag{2}$$

We used 16 peptides and, to save computational resources, the GB/SA implicit solvent model[55,56] in the ITS-enhanced MD simulation. The simulation was performed at 300 K with a spherical boundary condition (see the Supporting Information (SI) for detailed information) using the AMBER 9 software package[57] and FF96 all-atom force field[58,59] for a total time of about 1.5 μs. No cutoff was used in the simulation. In the present study, 80 (N = 80 in eq 1) evenly distributed temperatures between 243 and 343 K were used in the ITS-enhanced MD simulation.

Normal MD simulations were performed for a smaller number of (six) GGVVIA molecules, but with explicit TIP3P (model F[60]) solvent, using the AMBER 11 software package[61] and FF99SB force field.[62] In these simulations, peptides were immersed into a cubic box containing pure water (4056 water molecules) or 2 M NaCl solution (3750 water molecules, 153 Na^+ ions, and 153 Cl^- ions), respectively. Simulations for each solvent condition were run using an *NPT* ensemble at 300 K and 1 atm. A cutoff of 10.0 Å was applied for nonbonding interactions. Three independent trajectories, each with a simulation time of about 1.5 μs, were obtained in the pure water and NaCl solution, respectively.

In all simulations, the SHAKE algorithm[63] with a relative geometric tolerance of 10^{-5} was used to constrain all hydrogen bonds, and a time step of 2 fs was utilized.

We used the tLEaP module in the AMBER package to build the initial structure (Figure S1a in the SI) of peptide Aβ_{37-42}, the Armadillo C++ linear algebra library[64] for the transition matrix calculations in TPT, the VMD program package[65] for the visualization of molecular structures, and the Graphviz software toolkits[66] to draw the transition network graphs.

RESULTS

As shown in Figure 1, the ITS-enhanced sampling simulation allowed an efficient sampling in both energy and configuration spaces and led to efficient formation of various structures of Aβ_{37-42} molecules. As shown in Figure 1a, the potential energy distribution of the enhanced sampling simulation is much wider than that of the normal MD simulation. Moreover, we observed the reversible formation of Aβ_{37-42} oligomers, which include both aggregated and dispersed structures (Figure S1 in the SI). Starting from the initial structure (Figure S1a in the SI), the

dx.doi.org/10.1021/jp502169b | J. Phys. Chem. B XXXX, XXX, XXX−XXX

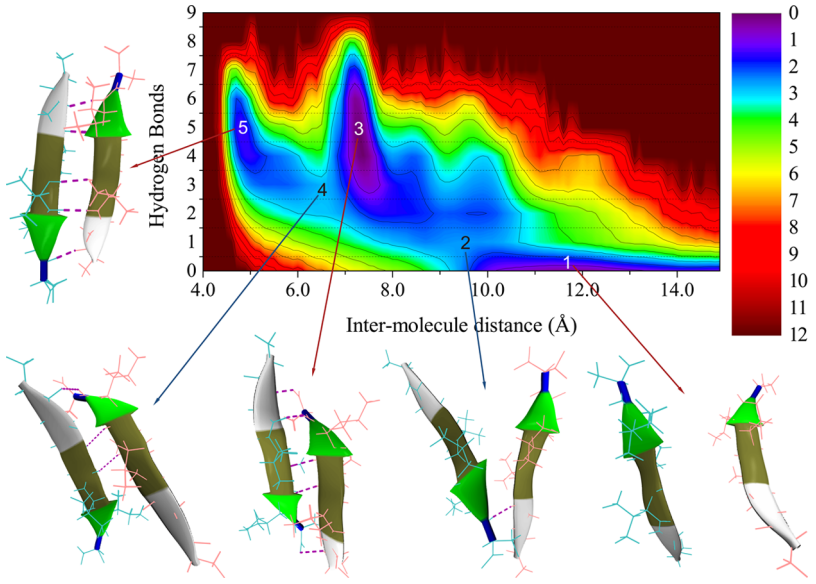

Figure 2. Free-energy landscape (in units of k_BT) and several typical snapshots for the association of polypeptide Aβ_{37-42} shown as a function of the number of hydrogen bonds as well as the average intermolecule distance. Regions 1, 3, and 5 form the basins in the landscape, and they represent the dispersed (region 1) and aggregated (regions 3 and 5) states of two molecules, respectively. Regions 2 and 4 are the energy barrier between regions 1 and 3 and the energy barrier between regions 3 and 5, respectively.

a)

Free Energy	Number of Contact Pairs						
Number of Hydrogen Bonds	6	5	4	3	2	1	0
10	-	-	18.78	-	-	-	-
9	-	15.25	10.80	-	-	-	-
8	6.42	3.82	7.43	-	-	-	-
7	4.12	2.74	5.82	6.32	-	-	-
6	2.94	**2.16**	4.19	5.24	-	-	-
5	2.57	**1.96**	3.09	4.33	6.47	7.88	-
4	2.51	**1.79**	2.42	3.55	5.28	6.67	-
3	2.80	**2.02**	**2.06**	2.90	4.27	5.50	-
2	3.48	2.55	**2.16**	**2.21**	3.35	5.03	-
1	4.51	3.43	2.69	**2.44**	2.70	3.70	-
0	5.86	4.62	3.72	3.12	2.92	2.65	**0.00**
Legend	0	3	6	9	12	15	18

b)

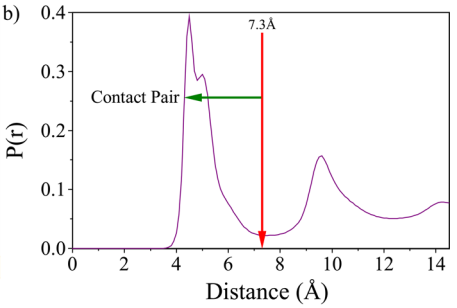

Figure 3. (a) Free-energy landscape (in units of k_BT) for the association of polypeptide Aβ_{37-42} shown as a function of the number of hydrogen bonds as well as the number of contact pairs. Different colors were used to indicate regions that closely resemble those shown in Figure 2. (b) Distribution function of the distance between two polypeptides.

peptides soon became fully dispersed (Figure S1b in the SI), and then, an aggregated structure containing multiple Aβ_{37-42} molecules was formed (Figure 1b). In fact, the transitions between aggregated and dispersed states occurred many times during the simulation, which means that our simulation reached equilibrium. Furthermore, we observed the formation of an aggregated structure containing 11 Aβ_{37-42} molecules (Figure 1b) without any bias applied toward aggregation. The aggregate structure of peptide Aβ_{37-42} with mixed parallel/antiparallel β-strands (with mainly antiparallel structures) is consistent with the polymorphism structure of Aβ_{37-42} from the MD simulation trajectories performed by Nguyen et al.,[31] which are dominantly antiparallel to each other but differ from the crystal structure.

On the basis of the ITS-enhanced sampling MD simulation, we calculated the free-energy landscape for polypeptide association and characterized the oligomer structures. First, we calculated the average intermolecular distance between a pair of peptides, defined as the averaged distance for the six closest pairs of residues, each from one of the two peptides. The distance between a pair of residues is defined as the distance between the mass centers of their backbone. The free energy was then drawn as a function of the average intermolecular distance d and the number of intermolecular hydrogen bonds h, $\Delta F(d,h) = -k_BT[\ln P(d,h) - \ln P_{max}]$. The calculated free energy F was reweighted using the weighting factor obtained by eq 2 ($\beta_0 = 1/k_BT_0$; $T_0 = 300$ K). A hydrogen bond is considered formed if the distance between the nitrogen and oxygen atoms is less than 3.5 Å and at the same time the ∠NHO angle is greater than 135°. The free-energy landscape and some typical snapshots are shown in Figure 2. In obtaining Figure 2, the entire simulations trajectory was used except for the first 50 ns. To test the convergence of data, the landscape was also calculated using the trajectory from 50 to 800 ns and is shown in Figure S2 in the SI. The results from both calculations are similar to each other. Distinct local minima can be seen on the free-energy landscape, regions 1, 3, and 5. Region 1 includes molecule pairs well separated, with large separation distances and no hydrogen bonds formed between them. Molecule pairs in region 3, with short distances and significant hydrogen bonding, form associated pairs. An energy barrier (marked as region 2 in the figure) is seen that separates regions 1 and 3. Due to the more suitable end-to-end antiparallel structures, molecule pairs in region 5 have similar numbers of hydrogen bonds but shorter intermolecular distances than those in region 3. Therefore, molecule pairs in region 5 are also consider

dx.doi.org/10.1021/jp502169b | J. Phys. Chem. B XXXX, XXX, XXX–XXX

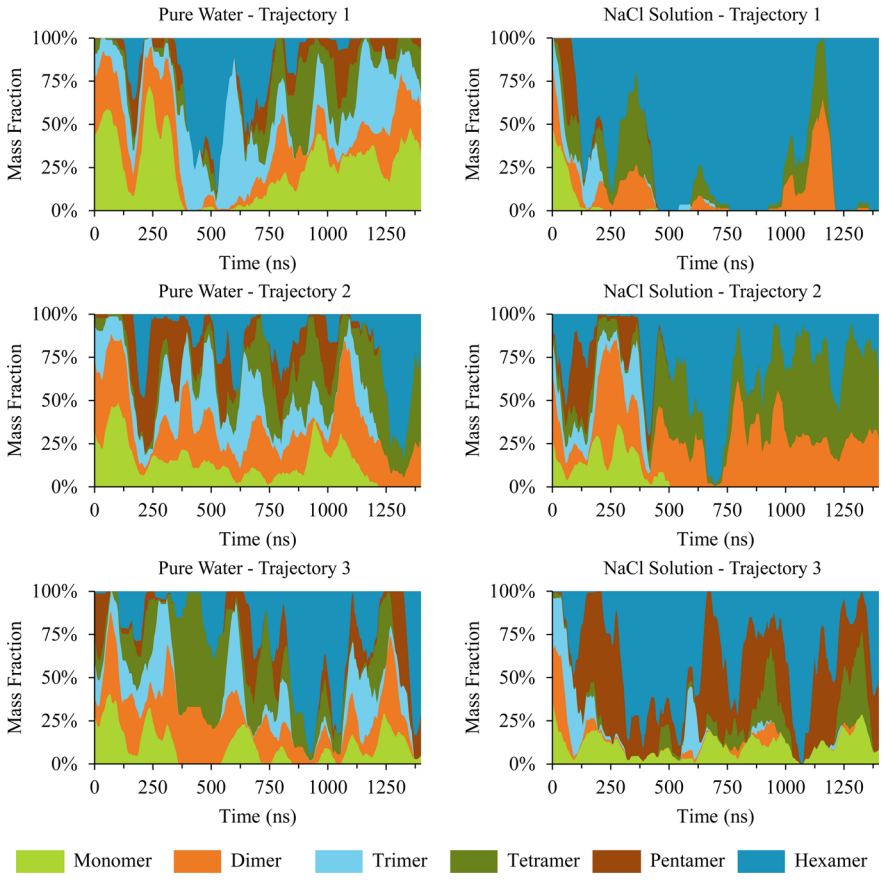

Figure 4. Fraction of each type of oligomer in explicit solutions as a function of time represented by stacked area charts.

associated. Furthermore, there also exists an energy barrier (region 4) between the two associated regions.

For convenience, the free-energy landscape for the association of a pair of polypeptides was also calculated as a function of the number of "contact pairs" c and the number of intermolecular hydrogen bonds h (Figure 3a). A contact pair is defined as a pair of interpeptide residues within a distance shorter than 7.3 Å. This distance corresponds to the lowest probability at the distribution of distances between two peptides of intermolecules (Figure 3b). Then, the free-energy landscape $\Delta F(c,h)$ was calculated in the same way as in the calculating of $\Delta F(d,h)$, with the same definition of hydrogen bond. As c and h are both integers, Figure 2b is conveniently used to determine whether two polypeptides are associated. According to the similar analysis used in Figure 2, block (0,0) (yellow frame) was defined as the "separated region", and the blocks of $c \geq 3$ and $d \geq 1$ (blue frame) were defined as the "associated region". Namely, a pair of polypeptides without contact pairs or intermolecular hydrogen bonds in between is considered separated, and a polypeptide pair with more than three contact pairs and one intermolecular hydrogen bond is considered associated. A polypeptide is considered to belong to a particular oligomer if it is associated with at least one of the polypeptides of that oligomer.

In the next step, we studied the kinetics of six $A\beta_{37-42}$ molecules in pure water and the NaCl solution. Using the criterion established above, a peptide is determined to belong to an aggregate (oligomer) or not. An analysis of all six peptides then allowed us to determine the aggregation state of the system, namely, the numbers of molecules in each oligomer (monomers, dimers, etc.). With this classification of the system, the trajectories from the normal MD simulations were analyzed to reveal the distribution of aggregate states as a function of the simulation time, as in shown in Figure 4. The results in this figures show that larger oligomers form more readily in the salt solution than in pure water, and thus, NaCl accelerates the aggregation of polypeptide and enhances the proportion of large oligomers. Two typical snapshots of the peptides obtained from the pure water and NaCl solution simulations are shown in Figure S3 in the SI, showing that the peptides in the NaCl solution favor the formation of the β-strand. It confirms experimental observations[35] that salt not only affects the populations but also the conformations of polypeptide aggregation. In addition, MD simulations of six $A\beta_{37-42}$ molecules in GB/SA implicit solvent were also performed using the AMBER FF96 force field to compare with the system in explicit solvent (Figure S4 in the SI). The fraction distribution of each type of oligomers in implicit solvent is similar to that of the corresponding system in explicit pure water (Figure 4), which validates the use of information obtained from implicit solvent simulation for the analysis of the simulation in explicit solvents.

To reveal the molecular mechanism of polypeptide aggregation, we employed the TPT[42,49] to analyze the pathways of $A\beta_{37-42}$ aggregation in solutions. A popular method[37] for building MSMs and to identify the long-lived, or metastable, states is first to divide the calculated structures into a large number of microstates based on their structural similarity and then merge the microstates together into metastable states. Another approach is to make use of the empirical "aggregate

dx.doi.org/10.1021/jp502169b | J. Phys. Chem. B XXXX, XXX, XXX−XXX

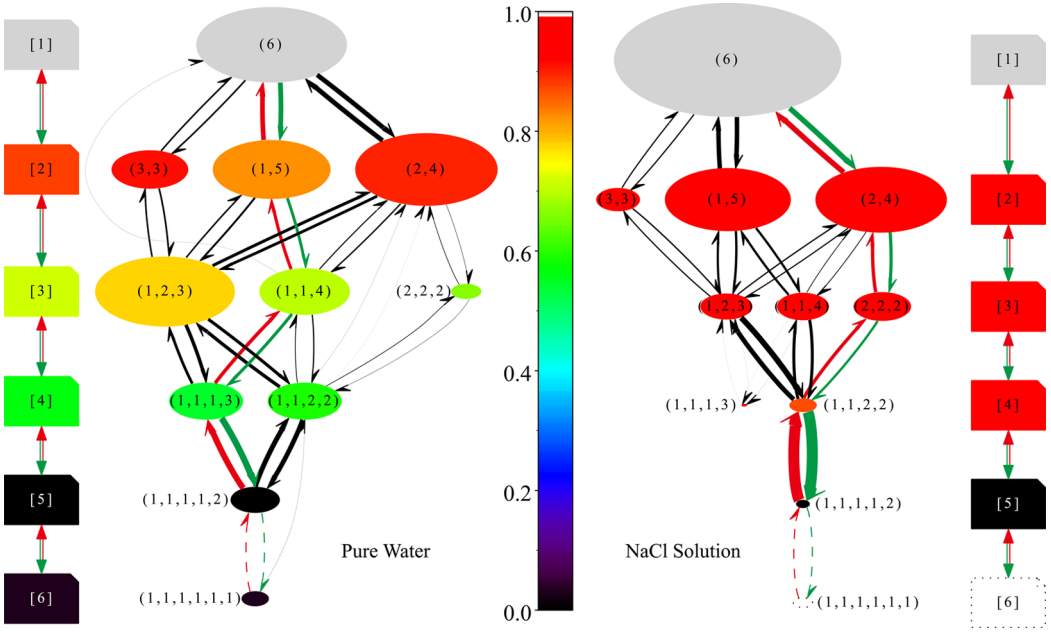

Figure 5. Transition network graphs of conformational states G for the aggregation of polypeptide Aβ_{37-42} in pure water and NaCl solution, respectively. The areas of nodes reflect their stationary distributions, the colors of the nodes refer to their forward committor probabilities, and the widths of the arrows represent the net fluxes (including both forward and backward). The dominant pathways of polypeptide aggregation and segregation are shown in red and green, respectively.

states",[46] which are defined based on the physical properties (especially, experimental observables) of the system. For polypeptide aggregation, one such structural property is the dispersion state of the polypeptides, namely, the distribution of oligomers of different sizes. In this method, we first separated the aggregate states formed by the six peptides into overall conformational states G, which contain totally 11 possible states (Figure 5). For example, the state containing two monomers and one tetramer is called [3](1,1,4), and the state that has one monomer and one pentamer is called [2](1,5) (see the SI for detailed information). This classification method reduces the number of states used in TPT; and the use of conformational states G allows us to analyze the aggregation pathway in a simple and intuitive way, namely, from the fully dispersed state [6](1,1,1,1,1,1) to the final aggregated state [1](6).

The beginning 250 ns of the simulations at each MD trajectory was excluded in the analysis. First, for each pair of states, the total transition number n_{ij} was calculated (Table S1 in the SI), where i and j represent two different conformational states. Our results show that the numbers of forward and backward transitions between a pair of states are approximately the same ($n_{ij} \approx n_{ji}$; see the SI for detailed information), which satisfies the requirement of detailed balance. Next, we calculated the interstate transition time t_{ij} by a simple approximation $t_{ij} = T_i/n_{ij}$, where T_i is the total lifetime of state i. Then, the Markovian transition matrix $P = (p_{ij})_{i,j\in G}$ and rate matrix $L = (l_{ij})_{i,j\in G}$ were constructed using the average transition time t_{ij}

$$p_{ij} = \frac{1}{t_{ij}} + \delta_{ij}\left(1 - \sum_{j\neq i} p_{ij}\right) \tag{3}$$

$$l_{ij} = \frac{1}{t_{ij}} - \delta_{ij} \sum_{j\neq i} l_{ij} \tag{4}$$

where δ_{ij} is the Kronecker delta function. Through diagonalization of the transition matrix P, the first left eigenvector π_i of each state i was calculated. As π_i is equivalent to the stationary distribution of state i, it is easily seen from these results (represented by the areas of each node in Figure 5) that NaCl increases the population of larger oligomers. Using the stationary distribution π_i, the time-reversed rate matrix $\tilde{L} = (\tilde{l}_{ij})_{i,j\in G}$ was then constructed

$$\tilde{l}_{ij} = \frac{\pi_i}{\pi_j} l_{ji} \tag{5}$$

The discrete committor probabilities were obtained from the matrices

$$\begin{cases} q_A^+ = 0 \\ q_B^+ = 1 \\ \sum_{j\in G} l_{ij} q_j^+ = 0 \qquad (i \neq A \text{ or } B) \end{cases} \tag{6}$$

$$\begin{cases} q_A^- = 1 \\ q_B^- = 0 \\ \sum_{j\in G} \tilde{l}_{ij} q_j^- = 0 \qquad (i \neq A \text{ or } B) \end{cases} \tag{7}$$

The discrete committor probabilities consist of both the forward committor q_i^+ and the backward committor q_i^-. The forward committor q_i^+ describes the probability of a state i transition to the final state B without reaching the initial state A first. Analogously, the backward committor q_i^- represents the transition probability from the initial state A to a state i without touching the final state B. Naturally, the fully dispersed state [6](1,1,1,1,1,1) would be the ideal initial state, and the final state B represents the fully aggregated state [1](6). (In this

dx.doi.org/10.1021/jp502169b | J. Phys. Chem. B XXXX, XXX, XXX−XXX

case, a state corresponding to a larger forward committor or a smaller backward committor has a higher transition probability to the final aggregated state than that to the dissociated states.) However, because the fully dispersed state [6](1,1,1,1,1,1) is rarely seen in the simulations in the NaCl solution (which indicates the easiness of polypeptide aggregation in the salt solution), we used the state [5](1,1,1,1,2) to represent the initial state A in this solution. The forward committors of each state in the two solutions are shown in Figure 5 using different colors to represent the value of the forward committor for each node. The figure exhibits that, in general, the forward committors of the states in NaCl soultion are largle than that in the pure water, which again shows that NaCl increases the tendency of the peptides to aggregate.

The probability current f_{ij}^{AB} of the reactive trajectory

$$f_{ij}^{AB} = \pi_i q_i^- l_{ij} q_i^+ (1 - \delta_{ij}) \tag{8}$$

which yields effectively the flux of transition $i \rightarrow j$ contributing to the process $A \rightarrow B$, was also calculated. Making use of the probability current, we obtained the net flux, which represents the net average number of reactive trajectories per time unit making a transition $i \rightarrow j$ on the way $A \rightarrow B$

$$f_{ij}^{+} = \max(f_{ij}^{AB} - f_{ji}^{AB}, 0) \tag{9}$$

In addition, the backward flux f_{ij}^{AB} and net flux f_{ij}^{-} were also calculated by a similar method (see the SI for detailed information). To illustrate the pathway of Aβ_{37-42} aggregation, the transition network composed of net fluxes is given in Figure 5.

Finally, the dominant pathway of Aβ_{37-42} aggregation was identified using an algorithm based on graph theory as proposed by E. Vanden-Eijnden et al.[49] In this scheme, a weighted digraph $G(S,E) = G\{f^+\}$ is constructed, where the vertex S is the set of all states in the conformational states G and the edge E is associated with the net fluxes $f^+ = (f_{ij}^+)$, $i_j \in G$. A reaction pathway $\omega = (i_0, i_1, ..., i_n)$, in $G(S,E)$, starting in vertex A and ending in vertex B, represents a reaction from state A to state B. According to TPT, the pathway ω is confined by the minimal net flux of a transition in the pathway. This flux is defined as the minimal current $c(\omega)$, and the edge with the minimal current is called the dynamical bottleneck (b_1,b_2) of pathway ω. The dominant pathway is the one including the maximal $c(\omega)$ in all pathways belonging to $G\{f^+\}$, marked by c_{max}. If $E_{sort} = (e_1, e_2, ..., e_{|E|})$ is the set of edges of $G\{f^+\}$ in ascending order by net fluxes, the edge e_m in E_{sort} is the bottleneck corresponding to c_{max} if and only if the subset $E'_{sort} = (e_m, e_{m+1}, ..., e_{|E|})$ contains a pathway from A to B but the subset $E''_{sort} = (e_{m+1}, e_{m+2}, ..., e_{|E|})$ does not. We used the depth-first search (DFS) algorithm[67] to seek the connected pathway in the subsets. The bottleneck corresponding to c_{max} was then found using the binary search algorithm.[68] Finally, the overall dominant pathway was identified by a recursive algorithm.[49]

The result obtained from the pathway search is shown in Figure 5. This figure demonstrates that the dominant pathway of Aβ_{37-42} aggregation changes with the solution conditions. The dominant pathway in pure water is [6](1,1,1,1,1,1) → [5](1,1,1,1,2) → [4](1,1,1,3) → [3](1,1,4) → [2](1,5) → [1](6), and the dominant pathway in the NaCl solution becomes [6](1,1,1,1,1,1) → [5](1,1,1,1,2) → [4](1,1,2,2) → [3](2,2,2) → [2](2,4) → [1](6). The discrepancy of transition networks in the two different solutions shows that NaCl promotes the aggregation of Aβ_{37-42} not only by accelerating the aggregation between molecules but also by changing the molecular mechanism of polypeptide association. For example, Aβ_{37-42} molecules prefer to form a dimer and aggregate among dimers in NaCl solution but not in pure water.

DISCUSSION AND CONCLUSION

In this paper, we presented a self-consistent strategy that was used to study the thermodynamics and kinetics for polypeptide aggregation using all-atom MD simulations. First, the free-energy landscape for polypeptide was obtained using the ITS-enhanced sampling method with implicit solvent models, which allows approximate but fast sampling of molecular configurations and thus identification of different aggregation states. Next, we performed normal MD simulations in explicit solvent to obtain "real dynamics" of polypeptide aggregation. Finally, the TPT was implemented to analyze the transition network and identify the dominant pathways of polypeptide aggregation.

In our simulations with the AMBER FF96 force field in implicit solvent, the aggregated single β-strands of peptide Aβ_{37-42} are dominantly antiparallel to each other. Similar structures were also obtained in the simulations using the AMBER FF99SB force field in both pure water and NaCl solution (Figure S3 in the SI). Although the polypeptide arrangement in these structures is different from that observed in the crystal structure,[18] the earlier MD simulations showed that the aggregation structures of peptide Aβ_{37-42} with antiparallel β-strands kept their aggregated architecture from disintegrating in water.[22] Moreover, Nguyen et al. suggested that peptide Aβ_{37-42} displays a packing polymorphism containing antiparallel β-strands, and the formation of antiparallel β-sheet character of Aβ_{37-42} oligomers is independent of the force field and the molecular dynamics software.[31]

According to Eisenberg et al.,[17,18,69] the polypeptide aggregation is stabilized by the interactions at the interface between the paired β-sheets consisting of the self-complementing hydrophobic side chains, the so-called steric zipper. For the peptide Aβ_{37-42}, the most favorable configuration of strands in a sheet to form a steric zipper is in parallel (Figure S6 in the SI). Moreover, Berryman et al.[22] have suggested that the antiparallel symmetries of β-strands are in general more stable than their parallel counterparts because of the formation of more hydrogen bonds and at the same time weaker electrostatic repulsion. For strongly hydrophobic sequences such as GGVVIA, the parallel between-strand arrangement can lead to favorable hydrophobic packing, overcoming their less favored hydrogen bonding and electrostatics interactions. We compare the conformational structures of the pair of peptides Aβ_{37-42} with the parallel and antiparallel β-strands in Figure S7 in the SI. The configuration of the parallel and antiparallel dimer of Aβ_{37-42} shows that, even when the two hydrogen bonds at the terminal residues are ignored, the number of interstrand hydrogen bonds between the antiparallel β-strands is still larger than that can be formed between a parallel pair. As mentioned above, the repulsion of the charged functional groups in the terminal ($-NH_3^+$ or $-COO^-$) is also expected to disturb the stability of the parallel β-strands. On the other hand, although the overlap of hydrophobic side chains of the antiparallel β-strands does exist along the fibril axis (Z direction in Figure S7c, SI), the overlapping area is obviously smaller than that of the parallel structure. In addition, to ensure the maximal number of hydrogen bonds between the antiparallel β-strands, the strand rotates along the Z-axis to form a small

dx.doi.org/10.1021/jp502169b | J. Phys. Chem. B XXXX, XXX, XXX−XXX

negative propeller angle. Therefore, the oligomers of the antiparallel Aβ_{37-42} peptides twist into a left-handed helix along the fibril axis (Figure1b). Chang et al. have shown that the structural stability of Aβ_{37-42} oligomers increases significantly when the number of β-sheets increases from single-layer to double-layer.[70] In fact, Nasica-Labouze et al.[71] and Nguyen et al.[31] used all-atom MD simulation to obtain the double-layer β-sheets of peptides GNNQQNY and GGVVIA, respectively. However, probably due to the relatively small number of polypeptides or the force field/implicit solvent model, only single-layer β-sheets of Aβ_{37-42} were observed in our simulations; the self-complementary effect of hydrophobic side chains cannot be embodied in the structures obtained here. It remains interesting to use all-atom simulations to investigate the formation of multilayer β-sheets of Aβ_{37-42} oligomers.

In this study, we made use of the ITS-enhanced sampling method in sampling configurations of polypeptide aggregation. The efficiency of ITS has been shown in studies for protein folding.[72−74] Here, using the ITS-enhanced simulations for a total simulation time of 1.5 μs, we obtained the Aβ_{37-42} oligomers including 11 peptides from dispersed monomers and the adequate data to obtain converged free-energy landscape. This study thus shows that the ITS-enhanced sampling method is also an effective method to study molecule self-assembly. On the basis of the ITS simulations, a self-consistent way was proposed to define the aggregation states of polypeptides using the calculated free-energy landscape. This method allowed us to classify the system into different conformational states G that were further used in pathway analyses. The pathway analyses performed based on the TPT yielded detailed transition networks of peptide Aβ_{37-42} aggregation in both pure water and NaCl solution (Figure 5).

The comparison of the transition networks in different solutions allowed us to assess the effect of NaCl on the aggregation process of peptide Aβ_{37-42}. The influence of NaCl on the mechanism of polypeptide aggregation exhibits the complexity of the self-assembly in solution and confirms experimental observations that salt not only affects the final structures but also kinetics of polypeptide aggregation.[35] A detailed analysis is ongoing to understand the molecular mechanism on how the salt affects the association between polypeptides in water.

■ ASSOCIATED CONTENT

Supporting Information

Details of the spherical boundary condition, conformational structures of Aβ_{37-42} in implicit solvent (Figure S1) as well as in explicit solvent (Figure S3), free-energy landscape calculated using the first 800 ns trajectory (Figure S2), fraction distribution in implicit solvent (Figure S4), list of conformational states G (Figure S5), transition numbers between each state (Table S1), details of equilibrium conditions as well as the backward committor in TPT, and molecule structures obtained from the crystal structure (Figure S6) as well as parallel/antiparallel β-strand pairs (Figure S7). This material is available free of charge via the Internet at http://pubs.acs.org.

■ AUTHOR INFORMATION

Corresponding Author

*E-mail: gaoyq@pku.edu.cn.

Notes

The authors declare no competing financial interest.

■ ACKNOWLEDGMENTS

We thank the National Program on Key Basic Research Project (973 Program, No. 2012CB917304) and the Natural Science Foundation of China (91027044 and 21125311) for financial support.

■ REFERENCES

(1) Lin, C. Y.; Gurlo, T.; Kayed, R.; Butler, A. E.; Haataja, L.; Glabe, C. G.; Butler, P. C. Toxic Human Islet Amyloid Polypeptide (h-IAPP) Oligomers Are Intracellular, and Vaccination to Induce Anti-Toxic Oligomer Antibodies Does Not Prevent h-IAPP-Induced Beta-Cell Apoptosis in h-IAPP Transgenic Mice. *Diabetes* **2007**, *56*, 1324−32.

(2) Irvine, G. B.; El-Agnaf, O. M.; Shankar, G. M.; Walsh, D. M. Protein Aggregation in the Brain: The Molecular Basis for Alzheimer's and Parkinson's Diseases. *Mol. Med.* **2008**, *14*, 451−464.

(3) Prelli, F.; Castano, E.; Glenner, G. G.; Frangione, B. Differences between Vascular and Plaque Core Amyloid in Alzheimer's Disease. *J. Neurochem.* **1988**, *51*, 648−651.

(4) Strittmatter, W. J.; Saunders, A. M.; Schmechel, D.; Pericak-Vance, M.; Enghild, J.; Salvesen, G. S.; Roses, A. D. Apolipoprotein E: High-Avidity Binding to Beta-Amyloid and Increased Frequency of Type 4 Allele in Late-Onset Familial Alzheimer Disease. *Proc. Natl. Acad. Sci. U.S.A.* **1993**, *90*, 1977−1981.

(5) Hensley, K.; Carney, J. M.; Mattson, M. P.; Aksenova, M.; Harris, M.; Wu, J. F.; Floyd, R. A.; Butterfield, D. A. A Model for Beta-Amyloid Aggregation and Neurotoxicity Based on Free Radical Generation by the Peptide: Relevance to Alzheimer Disease. *Proc. Natl. Acad. Sci. U.S.A.* **1994**, *91*, 3270−3274.

(6) Scheuner, D.; Eckman, C.; Jensen, M.; Song, X.; Citron, M.; Suzuki, N.; Bird, T. D.; Hardy, J.; Hutton, M.; Kukull, W.; et al. Secreted Amyloid β-Protein Similar to That in the Senile Plaques of Alzheimer'S Disease Is Increased in Vivo by the Presenilin 1 and 2 and APP Mutations Linked to Familial Alzheimer's Disease. *Nat. Med.* **1996**, *2*, 864−870.

(7) Mattson, M. P. Cellular Actions of Beta-Amyloid Precursor Protein and Its Soluble and Fibrillogenic Derivatives. *Physiol. Rev.* **1997**, *77*, 1081−1132.

(8) Lahiri, D. K.; Maloney, B. Beyond the Signaling Effect Role of Amyloid-β42 on the Processing of APP, and Its Clinical Implications. *Exp. Neurol.* **2010**, *225*, 51−54.

(9) Vivekanandan, S.; Brender, J. R.; Lee, S. Y.; Ramamoorthy, A. A Partially Folded Structure of Amyloid-Beta(1−40) In an Aqueous Environment. *Biochem. Biophys. Res. Commun.* **2011**, *411*, 312−316.

(10) Lambert, M. P.; Barlow, A. K.; Chromy, B. A.; Edwards, C.; Freed, R.; Liosatos, M.; Morgan, T. E.; Rozovsky, I.; Trommer, B.; Viola, K. L.; et al. Diffusible, Nonfibrillar Ligands Derived from Aβ1−42 Are Potent Central Nervous System Neurotoxins. *Proc. Natl. Acad. Sci. U.S.A.* **1998**, *95*, 6448−6453.

(11) Mucke, L.; Masliah, E.; Yu, G.-Q.; Mallory, M.; Rockenstein, E. M.; Tatsuno, G.; Hu, K.; Kholodenko, D.; Johnson-Wood, K.; McConlogue, L. High-Level Neuronal Expression of Aβ1−42 in Wild-Type Human Amyloid Protein Precursor Transgenic Mice: Synaptotoxicity without Plaque Formation. *J. Neurosci.* **2000**, *20*, 4050−4058.

(12) Chromy, B. A.; Nowak, R. J.; Lambert, M. P.; Viola, K. L.; Chang, L.; Velasco, P. T.; Jones, B. W.; Fernandez, S. J.; Lacor, P. N.; Horowitz, P.; et al. Self-Assembly of Aβ1−42 into Globular Neurotoxins. *Biochemistry* **2003**, *42*, 12749−12760.

(13) Li, H.; Monien, B. H.; Fradinger, E. A.; Urbanc, B.; Bitan, G. Biophysical Characterization of Aβ42 C-Terminal Fragments: Inhibitors of Aβ42 Neurotoxicity. *Biochemistry* **2010**, *49*, 1259−1267.

(14) Wu, C.; Murray, M. M.; Bernstein, S. L.; Condron, M. M.; Bitan, G.; Shea, J.-E.; Bowers, M. T. The Structure of Aβ42 C-Terminal Fragments Probed by a Combined Experimental and Theoretical Study. *J. Mol. Biol.* **2009**, *387*, 492−501.

(15) Yan, Y.; Wang, C. Aβ42 is More Rigid than Aβ40 at the C Terminus: Implications for Aβ Aggregation and Toxicity. *J. Mol. Biol.* **2006**, *364*, 853−862.

(16) Eisenberg, D.; Jucker, M. The Amyloid State of Proteins in Human Diseases. *Cell* **2012**, *148*, 1188−1203.
(17) Nelson, R.; Sawaya, M. R.; Balbirnie, M.; Madsen, A. O.; Riekel, C.; Grothe, R.; Eisenberg, D. Structure of the Cross-Beta Spine of Amyloid-Like Fibrils. *Nature* **2005**, *435*, 773−778.
(18) Sawaya, M. R.; Sambashivan, S.; Nelson, R.; Ivanova, M. I.; Sievers, S. A.; Apostol, M. I.; Thompson, M. J.; Balbirnie, M.; Wiltzius, J. J. W.; McFarlane, H. T.; et al. Atomic Structures of Amyloid Cross-Beta Spines Reveal Varied Steric Zippers. *Nature* **2007**, *447*, 453−457.
(19) Colletier, J.-P.; Laganowsky, A.; Landau, M.; Zhao, M.; Soriaga, A. B.; Goldschmidt, L.; Flot, D.; Cascio, D.; Sawaya, M. R.; Eisenberg, D. Molecular Basis for Amyloid-β Polymorphism. *Proc. Natl. Acad. Sci. U.S.A.* **2011**, *108*, 16938−16943.
(20) Fändrich, M.; Meinhardt, J.; Grigorieff, N. Structural Polymorphism of Alzheimer Aβ and Other Amyloid Fibrils. *Prion* **2009**, *3*, 89−93.
(21) Madine, J.; Jack, E.; Stockley, P. G.; Radford, S. E.; Serpell, L. C.; Middleton, D. A. Structural Insights into the Polymorphism of Amyloid-Like Fibrils Formed by Region 20−29 of Amylin Revealed by Solid-State NMR and X-ray Fiber Diffraction. *J. Am. Chem. Soc.* **2008**, *130*, 14990−15001.
(22) Berryman, J. T.; Radford, S. E.; Harris, S. A. Systematic Examination of Polymorphism in Amyloid Fibrils by Molecular-Dynamics Simulation. *Biophys. J.* **2011**, *100*, 2234−2242.
(23) Nguyen, H. D.; Hall, C. K. Molecular Dynamics Simulations of Spontaneous Fibril Formation by Random-Coil Peptides. *Proc. Natl. Acad. Sci. U.S.A.* **2004**, *101*, 16180−16185.
(24) Pellarin, R.; Caflisch, A. Interpreting the Aggregation Kinetics of Amyloid Peptides. *J. Mol. Biol.* **2006**, *360*, 882−892.
(25) Pellarin, R.; Guarnera, E.; Caflisch, A. Pathways and Intermediates of Amyloid Fibril Formation. *J. Mol. Biol.* **2007**, *374*, 917−924.
(26) Chebaro, Y.; Derreumaux, P. Targeting the Early Steps of Aβ16−22 Protofibril Disassembly by N-Methylated Inhibitors: A Numerical Study. *Proteins* **2009**, *75*, 442−452.
(27) Shea, J.-E.; Urbanc, B. Insights into Aβ Aggregation: A Molecular Dynamics Perspective. *Curr. Top. Med. Chem.* **2012**, *12*, 2596−2610.
(28) Mu, Y.; Gao, Y. Q. Self-Assembly of Polypeptides into Left-Handedly Twisted Fibril-Like Structures. *Phys. Rev. E* **2009**, *80*, 041927.
(29) Baftizadeh, F.; Biarnes, X.; Pietrucci, F.; Affinito, F.; Laio, A. Multidimensional View of Amyloid Fibril Nucleation in Atomistic Detail. *J. Am. Chem. Soc.* **2012**, *134*, 3886−3894.
(30) Baftizadeh, F.; Pietrucci, F.; Biarnes, X.; Laio, A. Nucleation Process of a Fibril Precursor in the C-Terminal Segment of Amyloid-Beta. *Phys. Rev. Lett.* **2013**, *110*, 168103.
(31) Nguyen, P. H.; Derreumaux, P. Conformational Ensemble and Polymorphism of the All-Atom Alzheimer's Aβ37−42 Amyloid Peptide Oligomers. *J. Phys. Chem. B* **2013**, *117*, 5831−5840.
(32) Chiti, F.; Webster, P.; Taddei, N.; Clark, A.; Stefani, M.; Ramponi, G.; Dobson, C. M. Designing Conditions for in Vitro Formation of Amyloid Protofilaments and Fibrils. *Proc. Natl. Acad. Sci. U.S.A.* **1999**, *96*, 3590−3594.
(33) Chiti, F.; Bucciantini, M.; Capanni, C.; Taddei, N.; Dobson, C. M.; Stefani, M. Solution Conditions Can Promote Formation of Either Amyloid Protofilaments or Mature Fibrils from the HypF N-Terminal Domain. *Protein Sci.* **2001**, *10*, 2541−2547.
(34) Zurdo, J.; Guijarro, J. I.; Jiménez, J. L.; Saibil, H. R.; Dobson, C. M. Dependence on Solution Conditions of Aggregation and Amyloid Formation by an SH3 Domain. *J. Mol. Biol.* **2001**, *311*, 325−340.
(35) Yoshimura, Y.; Lin, Y. X.; Yagi, H.; Lee, Y. H.; Kitayama, H.; Sakurai, K.; So, M.; Ogi, H.; Naiki, H.; Goto, Y. Distinguishing Crystal-Like Amyloid Fibrils and Glass-Like Amorphous Aggregates from Their Kinetics of Formation. *Proc. Natl. Acad. Sci. U.S.A.* **2012**, *109*, 14446−14451.
(36) Bowman, G. R.; Beauchamp, K. A.; Boxer, G.; Pande, V. S. Progress and Challenges in the Automated Construction of Markov State Models for Full Protein Systems. *J. Chem. Phys.* **2009**, *131*, 124101.
(37) Bowman, G. R.; Huang, X.; Pande, V. S. Using Generalized Ensemble Simulations and Markov State Models to Identify Conformational States. *Methods* **2009**, *49*, 197−201.
(38) Bowman, G. R.; Huang, X.; Pande, V. S. Network Models for Molecular Kinetics and Their Initial Applications to Human Health. *Cell Res.* **2010**, *20*, 622−630.
(39) Huang, X.; Bowman, G. R.; Bacallado, S.; Pande, V. S. Rapid Equilibrium Sampling Initiated from Nonequilibrium Data. *Proc. Natl. Acad. Sci. U.S.A.* **2009**, *106*, 19765−19769.
(40) Noé, F.; Krachtus, D.; Smith, J. C.; Fischer, S. Transition Networks for the Comprehensive Characterization of Complex Conformational Change in Proteins. *J. Chem. Theory Comput.* **2006**, *2*, 840−857.
(41) Noé, F.; Horenko, I.; Schütte, C.; Smith, J. C. Hierarchical Analysis of Conformational Dynamics in Biomolecules: Transition Networks of Metastable States. *J. Chem. Phys.* **2007**, *126*, 155102.
(42) Noé, F.; Fischer, S. Transition Networks for Modeling the Kinetics of Conformational Change in Macromolecules. *Curr. Opin. Struct. Biol.* **2008**, *18*, 154−162.
(43) Lu, Y.; Derreumaux, P.; Guo, Z.; Mousseau, N.; Wei, G. Thermodynamics and Dynamics of Amyloid Peptide Oligomerization Are Sequence Dependent. *Proteins* **2009**, *75*, 954−963.
(44) Matthes, D.; Gapsys, V.; Daebel, V.; de Groot, B. L. Mapping the Conformational Dynamics and Pathways of Spontaneous Steric Zipper Peptide Oligomerization. *PLoS One* **2011**, *6*, e19129.
(45) Paci, E.; Gsponer, J.; Salvatella, X.; Vendruscolo, M. Molecular Dynamics Studies of the Process of Amyloid Aggregation of Peptide Fragments of Transthyretin. *J. Mol. Biol.* **2004**, *340*, 555−569.
(46) Riccardi, L.; Nguyen, P. H.; Stock, G. Construction of the Free Energy Landscape of Peptide Aggregation from Molecular Dynamics Simulations. *J. Chem. Theory Comput.* **2012**, *8*, 1471−1479.
(47) Qiao, Q.; Bowman, G. R.; Huang, X. Dynamics of an Intrinsically Disordered Protein Reveal Metastable Conformations That Potentially Seed Aggregation. *J. Am. Chem. Soc.* **2013**, *135*, 16092−16101.
(48) Vanden-Eijnden, E. Transition Path Theory. In *Computer Simulations in Condensed Matter Systems: From Materials to Chemical Biology*, Ferrario, M., Ciccotti, G., Binder, K., Eds.; Springer-Verlag: Berlin, Germany, 2006; Vol. *703*, pp 453−493.
(49) Metzner, P.; Schutte, C.; Vanden-Eijnden, E. Transition Path Theory for Markov Jump Processes. *Multiscale Model. Simul.* **2009**, *7*, 1192−1219.
(50) Noé, F.; Schütte, C.; Vanden-Eijnden, E.; Reich, L.; Weikl, T. R. Constructing the Equilibrium Ensemble of Folding Pathways from Short off-Equilibrium Simulations. *Proc. Natl. Acad. Sci. U.S.A.* **2009**, *106*, 19011−19016.
(51) E, W.; Vanden-Eijnden, E. Transition-Path Theory and Path-Finding Algorithms for the Study of Rare Events. *Annu. Rev. Phys. Chem.* **2010**, *61*, 391−420.
(52) E, W.; Vanden-Eijnden, E. Towards a Theory of Transition Paths. *J. Stat. Phys.* **2006**, *123*, 503−523.
(53) Gao, Y. Q. An Integrate-over-Temperature Approach for Enhanced Sampling. *J. Chem. Phys.* **2008**, *128*, 064105.
(54) Gao, Y. Q. Self-Adaptive Enhanced Sampling in the Energy and Trajectory Spaces: Accelerated Thermodynamics and Kinetic Calculations. *J. Chem. Phys.* **2008**, *128*, 134111.
(55) Still, W. C.; Tempczyk, A.; Hawley, R. C.; Hendrickson, T. Semianalytical Treatment of Solvation for Molecular Mechanics and Dynamics. *J. Am. Chem. Soc.* **1990**, *112*, 6127−6129.
(56) Qiu, D.; Shenkin, P. S.; Hollinger, F. P.; Still, W. C. The GB/SA Continuum Model for Solvation. A Fast Analytical Method for the Calculation of Approximate Born Radii. *J. Phys. Chem. A* **1997**, *101*, 3005−3014.
(57) Case, D. A.; Darden, T. A.; Cheatham, T. E., III; Simmerling, C. L.; Wang, J.; Duke, R. E.; Luo, R.; Merz, K. M.; Pearlman, D. A.; Crowley, M.; et al. *AMBER 9*; University of California: San Francisco, CA, 2006.

(58) Kollman, P.; Dixon, R.; Cornell, W.; Fox, T.; Chipot, C.; Pohorille, A. The Development/Application of a 'Minimalist' Organic/Biochemical Molecular Mechanic Force Field Using a Combination of Ab Initio Calculations and Experimental Data. In *Computer Simulation of Biomolecular Systems: Theoretical and Experimental Applications*; van Gunsteren, W. F., Weiner, P. K., Wilkinson, A. J., Eds.; Kluwer: Dordrecht, The Netherlands, 1997; Vol. 3, pp 83−96.
(59) Cornell, W. D.; Cieplak, P.; Bayly, C. I.; Gould, I. R.; Merz, K. M.; Ferguson, D. M.; Spellmeyer, D. C.; Fox, T.; Caldwell, J. W.; Kollman, P. A. A Second Generation Force-Field for the Simulation of Proteins, Nucleic-Acids, and Organic-Molecules. *J. Am. Chem. Soc.* **1995**, *117*, 5179−5197.
(60) Price, D. J.; Brooks, C. L. A Modified TIP3P Water Potential for Simulation with Ewald Summation. *J. Chem. Phys.* **2004**, *121*, 10096−10103.
(61) Case, D.; Darden, T. A.; Cheatham, T. E., III; Simmerling, C.; Wang, J.; Duke, R.; Luo, R.; Crowley, M.; Walker, R.; Zhang, W.; et al. *AMBER 11*; University of California: San Francisco, CA, 2010.
(62) Hornak, V.; Abel, R.; Okur, A.; Strockbine, B.; Roitberg, A.; Simmerling, C. Comparison of Multiple Amber Force Fields and Development of Improved Protein Backbone Parameters. *Proteins* **2006**, *65*, 712−725.
(63) Ryckaert, J. P.; Ciccotti, G.; Berendsen, H. J. C. Numerical-Integration of Cartesian Equations of Motion of a System with Constraints - Molecular-Dynamics of N-Alkanes. *J. Comput. Phys.* **1977**, *23*, 327−341.
(64) Sanderson, C. *Armadillo: An Open Source C++ Linear Algebra Library for Fast Prototyping and Computationally Intensive Experiments*, Technical Report; NICTA: Australia, 2010.
(65) Humphrey, W.; Dalke, A.; Schulten, K. VMD: Visual Molecular Dynamics. *J. Mol. Graphics Modell.* **1996**, *14*, 33−38.
(66) Gansner, E. R.; North, S. C. An Open Graph Visualization System and Its Applications to Software Engineering. *Software Pract. Exper.* **2000**, *30*, 1203−1233.
(67) Tarjan, R. Depth-First Search and Linear Graph Algorithms. *SIAM J. Comput.* **1972**, *1*, 146−160.
(68) Lewis, G. N.; Boynton, N. J.; Burton, F. W. Expected Complexity of Fast Search with Uniformly Distributed Data. *Inform. Process. Lett.* **1981**, *13*, 4−7.
(69) Nelson, R.; Eisenberg, D. Recent Atomic Models of Amyloid Fibril Structure. *Curr. Opin. Struct. Biol.* **2006**, *16*, 260−265.
(70) Chang, L.-K.; Zhao, J.-H.; Liu, H.-L.; Liu, K.-T.; Chen, J.-T.; Tsai, W.-B.; Ho, Y. Molecular Dynamics Simulations to Investigate the Structural Stability and Aggregation Behavior of the GGVVIA Oligomers Derived from Amyloid β Peptide. *J. Biomol. Struct. Dyn.* **2009**, *26*, 731−740.
(71) Nasica-Labouze, J.; Meli, M.; Derreumaux, P.; Colombo, G.; Mousseau, N. A Multiscale Approach to Characterize the Early Aggregation Steps of the Amyloid-Forming Peptide GNNQQNY from the Yeast Prion Sup-35. *PLoS Comput. Biol.* **2011**, *7*, e1002051.
(72) Yang, L.; Shao, Q.; Gao, Y. Q. Thermodynamics and Folding Pathways of Trpzip2: An Accelerated Molecular Dynamics Simulation Study. *J. Phys. Chem. B* **2008**, *113*, 803−808.
(73) Yang, L.; Shao, Q.; Gao, Y. Q. Comparison between Integrated and Parallel Tempering Methods in Enhanced Sampling Simulations. *J. Chem. Phys.* **2009**, *130*, 124111.
(74) Zhang, C.; Ma, J. Enhanced Sampling and Applications in Protein Folding in Explicit Solvent. *J. Chem. Phys.* **2010**, *132*, 244101.